Accuracy of four-dimensional phase-contrast velocity mapping for blood flow visualizations: a phantom study.

Nilsson, Anders; Markenroth Bloch, Karin; Töger, Johannes; Heiberg, Einar; Ståhlberg, Freddy

Published in:
Acta Radiologica

DOI:
10.1177/0284185113478005

2013

Accuracy of four-dimensional phase-contrast velocity mapping for blood flow visualizations: a phantom study

Abstract

Background: Time-resolved three-dimensional, three-directional phase contrast magnetic resonance velocity mapping (4D PC-MRI) is a powerful technique to depict dynamic blood flow patterns in the human body. However, the impact of phase background effects on flow visualizations has not been thoroughly studied previously, and it has not yet been experimentally demonstrated to what degree phase offsets affect flow visualizations and create errors such as inaccurate particle traces.

Purpose: To quantify background phase offsets and their subsequent impact on particle trace visualizations in a 4D PC-MRI sequence. Additionally, we sought to investigate to what degree visualization errors are reduced by background phase correction.

Material and Methods: A rotating phantom with a known velocity field was used to quantify background phase of 4D PC-MRI sequences accelerated with SENSE as well as different k-t BLAST speedup factors. The deviation in end positions between particle traces in the measured velocity fields were compared before and after the application of two different phase correction methods.

Results: Phantom measurements revealed background velocity offsets up to 7 cm/s (7 % of velocity encoding sensitivity) in the central slice, increasing with distance from the center. Background offsets remained constant with increasing k-t BLAST speedup factors.
End deviations of up to 5.3 mm (1.8 voxels) in the direction perpendicular to the rotating disc were found between particle traces and the seeding plane of the traces. Phase correction by subtraction of the data from the stationary phantom reduced the average deviation by up to 56 %, while correcting the dataset with a first-order polynomial fit to stationary regions decreased average deviation up to 78 %.

Conclusion: Pathline visualizations can be significantly affected by background phase errors, highlighting the importance of dedicated and robust phase correction methods. Our results show that pathline deviation can be substantial if adequate phase background errors are not minimized.

Keywords: Phase errors, background phase correction, blood flow visualization, phase contrast imaging, velocity mapping

Phase-contrast velocity mapping with magnetic resonance imaging (PC-MRI) has become an important tool for quantifying and visualizing blood flow patterns in the human body (1-4). Dynamic velocity fields can be measured by three-dimensional time-resolved MR imaging sequences with velocity encoding in all three spatial directions, here denoted 4D PC-MRI. 4D PC-MRI has successfully been used to visualize blood flow and offers better understanding of physiology in different vascular regions (5-8).

However, clinical implementation of 4D PC-MRI is still limited by long acquisition times, and relatively low spatial and temporal resolution. Long scan times are trying for patients, and may result in changes of hemodynamic properties during examination. Well-known methods for reducing acquisition times are SENSitivity Encoding (SENSE) (9) and k-t BLAST (k-t Broad-use Linear Acquisition Speed-up Technique) (10). Both methods offer substantial time reduction by undersampling data in k-space and k-t space, respectively. Phase-contrast velocity mapping combined with undersampling techniques have been successfully used in a number of studies in conventional two-dimensional PC-MRI (2D PC-MRI) as well as in 4D PC-MRI (11-15).

All velocity measurements using phase contrast MR are prone to background phase errors, which may vary in space as well as in time. Background phase is caused by e.g. concomitant gradients, by non-compensated eddy currents caused by different eddy current behavior in the velocity encoding segments, and by nonlinearities in the applied magnetic field gradients (16). It should in this context be noted that in 4D PC-MRI velocity encoding is made in all directions over a large volume rather than in one direction in a selected slice as is the case for 2D-PC MRI.

Background effects can be expected to propagate into flow visualizations such as pathlines and streamlines that are based on integration of the acquired velocity field, as phase errors

accumulate during each integration step. A small phase error can therefore inflict a large deviation in the resulting particle path (17). Background phase corrections of 4D PC-MRI datasets are therefore generally a necessity in modern scanners in order to get reliable, reproducible and quantitative velocity information over a larger region of the field of view (FOV). For the effects of concomitant gradients, analytical solutions can be found and adequate correction methods can be implemented (18). Eddy current induced errors can be partly corrected by applying pre-emphasis on the gradients, but remaining errors need to be dealt with using post processing.

In spite of the large amount of promising applications for 4D PC-MRI, investigations of the accuracy of the technique are primarily done by comparing quantitative flow values by 4D PC-MRI with traditional 2D PC-MRI measurements, regarding 2D PC-MRI as gold-standard (19-22). While the impact of velocity noise on flow visualizations has recently been studied (23), the quantitative effects of phase offsets in flow visualizations remain to a large extent unexplored.

Furthermore, for residual linear as well as non-linear phase errors, two of the most commonly used correction methods are subtraction of the acquired velocity data with velocity data acquired by an identical pulse sequence on a static phantom (24, 25), and fitting a polynomial function to the velocity in static regions in the FOV (26, 27).

Therefore, the aim of this study was to investigate the effects of two background phase correction methods for undersampled 4D-PC MRI on flow visualization accuracy in a rotating phantom model. The two correction methods chosen, being two of the most commonly used clinical methods, were i) subtraction of background phase using a dataset from a static phantom, and ii) a first-order background correction based on a three-dimensional fit of phase in static regions.

Material and Methods

Phantom setup

To investigate phase background effects in 4D PC-MRI sequences, a rotating phantom was constructed. A rotating phantom provides a well-defined, continuous linear distribution of velocities (28). The phantom was constructed of three plastic cylindrical compartments (diameter 20 cm, thickness of central cylinder 4.5 cm, thickness of outer cylinders 3.5 cm, giving a total volume of 20×20×20 cm^3), placed parallel to each other and connected by a center axis (Fig. 1). All compartments were filled with agarose gel (Agarose type VI, Sigma-Aldrich Sweden AB, Stockholm, Sweden) with 0.9 % saline content and doped with $NiSO_4$ to give relaxation times similar to myocardium. The compartments were sealed with silicone to prevent the gel from drying. While the two outer compartments remained static, the center cylinder could be set into rotation using compressed air from a nozzle. The outer compartments provided static regions for subsequent phase background corrections, as well as stabilization of the phantom from possible vibrations while the center cylinder was rotating. The phantom (Fig. 1) was positioned in the isocenter of the MR scanner with the rotating cylinder in the x-z plane (Right-Left, Feet-Head plane), and its rotational axis pointing upward along the y (Anterior-Posterior) direction, perpendicular to the B_0-field (z-direction). A photoelectric cell mounted on the phantom provided an electric pulse for each revolution of the center cylinder, and this pulse was fed into the MR scanner via the PPU unit for triggering of the data acquisition. The rotational frequency (average ±maximum variation) of the phantom disc during all sequences was 60±3 revolutions per minute (RPM), corresponding to a velocity of 62±3 cm/s at the edges of the rotating cylinder.

Data acquisition

All measurements were performed on a 3T Achieva MR scanner (Philips Medical Systems, Best, The Netherlands) with a six-channel cardiac receive coil. The sequence used was a segmented 3D TFE (Turbo Field Echo) radiofrequency- and gradient-spoiled sequence with a Hadamard four-point velocity encoding strategy using a maximal gradient strength of 20 mT m^{-1} and a gradient slew rate of 100 mT $m^{-1}ms^{-1}$ (29, 30). Further sequence parameters were: Field-of-view = 240×240×210 mm^3, matrix size = 80×80×70, 20 acquired timeframes, TE/TR=3.0/5.2 ms, temporal resolution = 41.4 ms, flip angle = 8 degrees, and isotropic velocity encoding strength (VENC) of 100 cm/s. The scans were prospectively triggered by the photocell signal via the PPU interface. Four different versions of this sequence were investigated, each acquired with a different acceleration strategy consisting of either SENSE with a speedup factor of 2, or k-t BLAST with speedup factors of 2, 4 and 5, respectively. The imaging stack was positioned coronally with the slice-encoding direction parallel to the y direction. The acquisition time for the datasets were 29 minutes (SENSE = 2), 29 minutes (k-t = 2), 15 minutes (k-t = 4) and 12 minutes (k-t = 5). For each timeframe, two phase encoding steps were acquired, in which velocity encoding in four segments were executed, resulting in a segmentation factor of 2. The phase encoding lines in k-space were collected linearly, such that each phase encoding line was collected after the nearest lower profile. All sequences were executed twice; once with the central cylinder rotating (rotating mode), and once when the central cylinder of the phantom was at rest (static mode).

Quantification of measured velocities

To quantify the background phase velocity, root-mean-square (RMS) velocity maps in the static central compartment (acquired during the static mode) were calculated voxel-by-voxel as

$$v_{rms} = \sqrt{\frac{1}{N}\sum_{i=1}^{N}\left(v_{x,i}^2 + v_{y,i}^2 + v_{z,i}^2\right)}, \quad (1)$$

where *N* is the number of acquired timeframes, in our case N = 20. Matlab R2008b (Mathworks Inc., Natick, Massachusetts, U.S.A.) was used for image evaluation. In the central slice, located in the central part of the middle compartment, velocities in each velocity direction (v_x,v_y and v_z) were time-averaged over all dynamic frames and plotted as line profiles in x- and z-direction. The velocity of voxels with magnitude values lower than 15 % of the maximum magnitude value was set to zero in all velocity directions prior to evaluation.

Background phase corrections

The built-in Maxwell correction was active during all sequences (18). Since the phase-correction method for eddy-current effects provided by the vendor was not optimized for phantom imaging or 4D PC-MRI sequences, this correction was not applied.

Residual background corrections were made using two methods. The first method consisted of subtracting the dataset acquired during rotating mode with a corresponding dataset acquired during static mode. The second method consisted of fitting a first-order polynomial to the background velocity field in the static parts of the FOV in the rotating-mode datasets, and subtracting the resulting polynomial from the acquired data. The polynomial fit was performed for each velocity direction independently.

The static parts in the image volume were automatically identified in two steps. In the first step, voxels with a magnitude value exceeding 10 % of the maximum intensity were selected. Of the selected voxels, those with velocity magnitude lower than 6 cm/s were considered as stationary voxels and used for fitting a first-order polynomial function for each velocity direction by least-squares fitting performed in Matlab. The fit was performed separately for each time frame and velocity direction.

The datasets acquired during rotating mode were investigated with respect to effects on flow visualizations a) before any corrections, b) after subtraction of the corresponding static dataset acquired while the phantom was at rest , and c) after background phase corrections by means of automatically fitting the 1st order (linear) polynomial to the static parts in the FOV.

Effects on flow visualizations

To study the influence on flow visualizations, the acquired datasets were exported to the visualization software GTFlow v.1.6.8 (Gyrotools Ltd, Zurich, Switzerland) for particle trace visualization. Pathlines were created by emitting 2673 equally-spaced particles from a plane positioned perpendicular to the rotational axis in the center of the rotating disc. The diameter of the emitting plane was approximately 20 % smaller than the cylinder dimensions in order to avoid partial-volume effects at the edges of the cylinder. The particles were traced over all 20 timeframes.

The pathline data were exported from GTFlow and imported into Matlab, where each particle trace was compared to the corresponding particle trace in the phase-corrected datasets, originating from the same starting point. The resulting absolute deviation in the y direction from the seeding plane of the particle traces (Δy) in the measured, subtracted and phase corrected datasets were compared. The absolute deviation Δy from the seeding plane was also calculated for particle traces originating from seven 10 mm wide radius intervals, starting at 10 mm distance from the rotational center.

Statistics

Average absolute deviation in the y (AP) direction (Δy) of the end positions was calculated for all particle traces (n=2673) in each dataset along with the standard deviation, and compared to the corrected datasets, as well as between the two correction methods, by a two-

sided dependent (paired) t-test. The same statistical test was used to evaluate whether the average deviation in each radius interval were significantly different after either subtraction or linear phase correction, compared to the non-corrected datasets. In the statistical evaluations, the level of significance was chosen as $p<0.05$.

Results

Static acquisitions

RMS velocity maps from the central compartment of the static acquisitions are presented in Fig. 2. For all 4D PC-MRI sequences, the RMS background velocity was below 2 cm/s in the center of FOV, increasing towards the periphery of the disc to approximately 7 cm/s. The RMS background velocity had a similar pattern for all sequences, increasing towards the edges of the central cylinder. The highest RMS velocity was seen near the right edge of the central cylinder (Fig. 2). With the exception of a small area in the lower part of the phantom for the k-t=2 dataset, no marked differences in phase background for the k-t BLAST accelerated datasets compared to the SENSE-accelerated dataset were seen (Fig. 2 E-F). Of notice is the position of the photocell in the lower left corner of the disc, which may have interfered with the magnetic field, creating image artifacts. Fig. 3 presents corresponding time-averaged velocity components (v_x, v_y and v_z) from the same line profiles as used in Fig. 2. All sequences were found to have similar patterns of background velocity offsets. The v_x (RL) velocity component was found to vary the most over the phantom disc (from +2 cm/s to -6 cm/s), with the highest deviation towards the right side of the disc, in accordance with the RMS velocity offsets presented in Fig. 2.

Rotating acquisitions

Fig. 4 A-C shows measured time-averaged velocities in the rotating central compartment, acquired with the SENSE-accelerated 4D sequence. As expected, a linear phase behavior is dominant in the x and z directions, however, similar velocity offsets in the direction perpendicular to the rotation (y-direction) were seen for both datasets, as well as a higher phase offset in the lower left corner, close to the photocell.

Fig. 4 D presents the time-averaged velocity component $v_{y,}$ (perpendicular to the rotational velocity), acquired with the SENSE-accelerated sequence, along a line profile in the z direction for the uncorrected and the two corrected cases. In all cases, the measured v_y velocity component increased with z position, while both correction methods decreased the average velocity offset, with the highest reduction in the central parts of the disc. The linear fitting method could be seen to over-compensate phase offsets at the left part of the cylinder, resulting in negative velocities. For the line profiles presented in Fig. 4 D, average absolute velocity along the line profile was 0.7 cm/s for the rotating dataset, 0.6 cm/s for the subtracted dataset, and 0.5cm/s for the linear corrected dataset.

Pathline analysis

For all datasets, pathlines created in the acquired velocity field of the rotating cylinder were found to deviate from the seeding plane. An example is given in Fig. 5, which shows a typical pathline trajectory in the dataset acquired with SENSE, before and after background phase corrections. Average absolute pathline endpoint deviation in the y direction from the seeding plane in the acquired, uncorrected datasets was found to be similar across the sequence types, with an average Δy ranging between 5.0 and 5.3 mm as shown in Table 1.

The average absolute pathline endpoint deviation from the seeding plane was significantly reduced after subtraction with the static datasets for all sequence types (remaining deviation

ranging between 2.2 mm and 2.7 mm), and the reduction in deviation was statistically significant for all sequence types.

Likewise, for all sequence types, the deviation significantly decreased after linear phase correction (remaining deviation ranging between 1.1 mm and 1.5 mm), and there was a significant difference between the reduction obtained using the subtraction and the linear correction method. Comparisons between the SENSE-accelerated data set and the k-t accelerated data sets for the two correction methods showed significant differences in two cases (SENSE vs. k-t=2, subtracted data and SENSE vs. k-t=4, linearly corrected data), but were not significant for all other cases.

The average Δy of the seeded pathlines, broken down into 10 mm intervals from the rotational center, is presented in Fig. 6. Error bars represent ±SD. In general, average deviation in end positions was constant throughout the radius of the disc for all sequences used. Both correction methods resulted in statistically significant reductions in Δy compared to the non-corrected datasets for all sequences and intervals, and the linearly corrected datasets showed a higher reduction in deviation compared to the subtracted datasets.

Discussion

Phase errors can be expected to affect pathline and streamline visualizations, because of the accumulation of phase errors throughout the particle trace. Our results show that even in a constant velocity field created by a rotating disc, deviations of particle trace trajectories from the seeding plane of up to 5.3 mm (1.8 voxels) may occur during the duration of a typical heartbeat. Given the size of the vessels close to the heart, this could result in pathlines seeded from within the vessels extending beyond the vessel border, failing to depict the correct physiology.

The same amount of deviation from the seeding plane was observed close to the isocenter of the magnet as in more distant parts of the rotating disc, indicating that the phase background offsets were not even negligible in the magnet isocenter.

Contributions to the background phase offsets can be related to a number of sources, including gradient nonlinearities, eddy-currents and concomitant gradient fields (16, 18). In this work, we evaluated improvements in pathline accuracy after two simple phase background correction methods. Subtraction with a static dataset significantly reduced the particle trace deviation. Linear background correction was also found to reduce particle trace deviation, with superior results compared to the subtraction method. The significant reduction of the difference in end position of the particle traces obtained after phase correction by these methods points at the importance to perform phase background corrections, also after compensation for concomitant gradient effects.

It is important to notice that the subtraction method increases the amount of noise in the phase-corrected datasets by a factor $\sqrt{2}$. A higher amount of noise can be expected to increase pathline deviations (17). In our case, the subtraction method presented a higher average deviation as well as dispersion compared to the linearly corrected datasets, and this noise amplification may be a reason for the observed superiority of the linear fit method. In this work, we chose to only use a first-order background correction, as this low-order polynomial order has been found to be appropriate for reducing phase offsets *in-vivo* (27). The linear background fit did sometimes overcompensate the background phase offsets, leading to net velocity offsets in different parts of the phantom. This effect could be explained by the fact that the phase background in our phantom experiments was not entirely linear, which suggests that a higher-order phase correction method could be useful. The significant improvement seen with our low-order correction can partly be explained by the built-in Maxwell correction, which was active during imaging, indicating that a combination of Maxwell correction and

linear fitting is advantageous. We also investigated the combination of both subtraction and linear phase correction, and found that it failed to reduce the average deviation further, compared to only using one of the phase correction methods. This result is expected, as the linear phase offsets in the static parts of the FOV have been reduced to a large extent after subtraction, leaving less phase offset for the fitting procedure to work with.

In spite of these results obtained in a phantom geometry, it should be noted that phase background correction in the clinical setting is expected to be more difficult compared to the phantom case, as cardiac imaging is affected by error sources such as respiration and motion artifacts, triggering errors, patient motion and B_1- as well as B_0- inhomogeneities. Although the subtraction method has been suggested for clinical use, it may not be practical because of the need to acquire two datasets (24). Furthermore, the subtraction was in this work performed between identical objects and geometries, which is not possible in the clinical setting and where it is instead performed between the imaged object and static phantoms.

The linear fitting background correction method used in this work resulted in encouraging correction results; however it requires static regions, which in cardiac imaging usually are located at a large distance from the heart in the outer parts of the FOV. In combination with the error sources previously mentioned, fitting a polynomial function to static regions, especially of higher order, can be difficult. In this work, we used an automatic selection using two critera to define static regions: a minimum magnitude signal threshold, and a maximum velocity magnitude threshold. Additional criterions could be added when performing background correction in vivo, such as setting a threshold of the velocity variation over time (27, 31).

In spite of drawbacks with the simple background correction methods described, our results show that phase correction by either subtracting the acquired velocity field with an identical dataset of a static object, or correcting the acquired velocity field with a first-order, time-

dependent polynomial fit to the phase background in static regions reduces the deviation of particle traces from their true trajectory. The results further indicate that significant improvements are made in the depiction of flow patterns after background phase offsets have been reduced.

Since both the subtraction method and the linear phase correction leave some velocity-dependent phase errors uncorrected, requiring additional correction after acquisition (32), further work includes evaluation of the use of more advanced background correction methods, such as higher-order polynomial corrections.

There are some limitations of this study. As k-t BLAST reconstructions results in undersampling of k-t space, rapid velocity alterations are expected to be blurred throughout time (10, 12). Recent studies with 4D PC combined with k-t BLAST have indicated underestimated peak- and flow velocities, and problems of depicting more complex flow patterns (14, 21).Owing to the phantom construction, this effect could not be assessed with the present phantom study.

A second limitation with our phantom setup is the uncertainty of the velocity in the rotating plane of the disc during operation. We therefore measured all deviation distances perpendicular to the rotating plane. It should be noted however, that the velocity variation (approximately five percent) is in the order of the expected variation in heart rate during a clinical PC-MRI scan. Simulating pathlines in datasets with rotational velocities between the maximal and minimal recorded RPM values, we found that the average total difference of end position in the rotating plane became over 20 mm, increasing with radial distance, indicating that pathline uncertainties in vivo can be substantial in spite of background correction efforts. The phantom had static parts in only one direction (y), which could have affected the background fitting method. It should be noted however, that there is also a lack of static

regions around the cardiac area in clinical imaging. Furthermore, we compared the fit obtained as described in the method section with a fit made from all three phantom compartments in static mode, and no substantial differences were observed.
Finally, the photocell mounted on the phantom may have created additional phase offsets, which may explain that the RMS background velocities were seen to increase towards the position of the photocell for all sequences. Furthermore, the "hotspots" observed in some of the datasets are positioned in the same position as the photocell.

In conclusion, the present work shows that phase errors can cause pathlines to deviate substantially from the correct path plane, indicating that caution should be used when interpreting particle trace visualizations. The results also highlight that background phase errors have to be taken into consideration and corrected for, when quantitative pathline analysis is performed.

Declaration of interests

KMB is employed by Philips Healthcare. The other authors declare that they have no competing interests.

Acknowledgements

The authors would like to thank Gert-Inge Jönsson, for his contribution in the construction and design of the rotating phantom.

References

1. Kilner PJ, Yang GZ, Wilkes AJ*, et al.* Asymmetric redirection of flow through the heart. *Nature* 2000;**404**:759-61
2. Kilner PJ, Yang GZ, Mohiaddin RH*, et al.* Helical and retrograde secondary flow patterns in the aortic arch studied by three-directional magnetic resonance velocity mapping. *Circulation* 1993;**88**:2235-47

3. Markl M, Harloff A, Bley TA*, et al.* Time-resolved 3D MR velocity mapping at 3T: improved navigator-gated assessment of vascular anatomy and blood flow. *J Magn Reson Imaging* 2007;**25**:824-31
4. Kvitting JP, Ebbers T, Wigstrom L*, et al.* Flow patterns in the aortic root and the aorta studied with time-resolved, 3-dimensional, phase-contrast magnetic resonance imaging: implications for aortic valve-sparing surgery. *J Thorac Cardiovasc Surg* 2004;**127**:1602-7
5. Wigstrom L, Ebbers T, Fyrenius A*, et al.* Particle trace visualization of intracardiac flow using time-resolved 3D phase contrast MRI. *Magn Reson Med* 1999;**41**:793-9
6. Kozerke S, Hasenkam JM, Pedersen EM*, et al.* Visualization of flow patterns distal to aortic valve prostheses in humans using a fast approach for cine 3D velocity mapping. *J Magn Reson Imaging* 2001;**13**:690-8
7. Markl M, Kilner PJ, Ebbers T. Comprehensive 4D velocity mapping of the heart and great vessels by cardiovascular magnetic resonance. *J Cardiovasc Magn Reson* 2011;**13**:7
8. Frydrychowicz A, Francois CJ, Turski PA. Four-dimensional phase contrast magnetic resonance angiography: potential clinical applications. *Eur J Radiol* 2011;**80**:24-35
9. Pruessmann KP, Weiger M, Scheidegger MB*, et al.* SENSE: sensitivity encoding for fast MRI. *Magn Reson Med* 1999;**42**:952-62
10. Tsao J, Boesiger P, Pruessmann KP. k-t BLAST and k-t SENSE: dynamic MRI with high frame rate exploiting spatiotemporal correlations. *Magn Reson Med* 2003;**50**:1031-42
11. Kozerke S, Tsao J, Razavi R*, et al.* Accelerating cardiac cine 3D imaging using k-t BLAST. *Magn Reson Med* 2004;**52**:19-26
12. Baltes C, Kozerke S, Hansen MS*, et al.* Accelerating cine phase-contrast flow measurements using k-t BLAST and k-t SENSE. *Magn Reson Med* 2005;**54**:1430-8
13. Marshall I. Feasibility of k-t BLAST technique for measuring "seven-dimensional" fluid flow. *J Magn Reson Imaging* 2006;**23**:189-96
14. Stadlbauer A, van der Riet W, Crelier G*, et al.* Accelerated time-resolved three-dimensional MR velocity mapping of blood flow patterns in the aorta using SENSE and k-t BLAST. *Eur J Radiol* 2010;**75**:e15-e21
15. Thunberg P, Karlsson M, Wigstrom L. Accuracy and reproducibility in phase contrast imaging using SENSE. *Magn Reson Med* 2003;**50**:1061-8
16. Higgins CB, Roos Ad. MRI and CT of the cardiovascular system. 2nd ed. Philadelphia, Pa.: Lippincott Williams & Wilkins; 2006. 656 p. p.
17. Napel S, Lee DH, Frayne R*, et al.* Visualizing three-dimensional flow with simulated streamlines and three-dimensional phase-contrast MR imaging. *J Magn Reson Imaging* 1992;**2**:143-53
18. Bernstein MA, Zhou XJ, Polzin JA*, et al.* Concomitant gradient terms in phase contrast MR: analysis and correction. *Magn Reson Med* 1998;**39**:300-8
19. Markl M, Chan FP, Alley MT*, et al.* Time-resolved three-dimensional phase-contrast MRI. *J Magn Reson Imaging* 2003;**17**:499-506
20. Stalder AF, Russe MF, Frydrychowicz A*, et al.* Quantitative 2D and 3D phase contrast MRI: optimized analysis of blood flow and vessel wall parameters. *Magn Reson Med* 2008;**60**:1218-31
21. Carlsson M, Toger J, Kanski M*, et al.* Quantification and visualization of cardiovascular 4D velocity mapping accelerated with parallel imaging or k-t BLAST: head to head comparison and validation at 1.5 T and 3 T. *J Cardiovasc Magn Reson* 2011;**13**:55
22. Brix L, Ringgaard S, Rasmusson A*, et al.* Three dimensional three component whole heart cardiovascular magnetic resonance velocity mapping: comparison of flow measurements from 3D and 2D acquisitions. *J Cardiovasc Magn Reson* 2009;**11**:3

23. Friman O, Hennemuth A, Harloff A*, et al.* Probabilistic 4D blood flow tracking and uncertainty estimation. *Med Image Anal* 2011;**15**:720-8
24. Chernobelsky A, Shubayev O, Comeau CR*, et al.* Baseline correction of phase contrast images improves quantification of blood flow in the great vessels. *J Cardiovasc Magn Reson* 2007;**9**:681-5
25. Kilner PJ, Gatehouse PD, Firmin DN. Flow measurement by magnetic resonance: a unique asset worth optimising. *J Cardiovasc Magn Reson* 2007;**9**:723-8
26. Walker PG, Cranney GB, Scheidegger MB*, et al.* Semiautomated method for noise reduction and background phase error correction in MR phase velocity data. *J Magn Reson Imaging* 1993;**3**:521-30
27. Lankhaar JW, Hofman MB, Marcus JT*, et al.* Correction of phase offset errors in main pulmonary artery flow quantification. *J Magn Reson Imaging* 2005;**22**:73-9
28. Nordell B, Stahlberg F, Ericsson A*, et al.* A rotating phantom for the study of flow effects in MR imaging. *Magn Reson Imaging* 1988;**6**:695-705
29. Dyverfeldt P, Kvitting JP, Sigfridsson A*, et al.* Assessment of fluctuating velocities in disturbed cardiovascular blood flow: in vivo feasibility of generalized phase-contrast MRI. *J Magn Reson Imaging* 2008;**28**:655-63
30. Pelc NJ, Bernstein MA, Shimakawa A*, et al.* Encoding strategies for three-direction phase-contrast MR imaging of flow. *J Magn Reson Imaging* 1991;**1**:405-13
31. Ebbers T DP, Sigfridsson A, Warntjes M, Wigström L. Higher order weighted least-squares phase offset correction for improved accuracy in phase-contrast MRI. *Proceedings of the 16th Annual Meeting of ISMRM, Toronto*; 2008:abstract 1367.
32. Markl M, Bammer R, Alley MT*, et al.* Generalized reconstruction of phase contrast MRI: analysis and correction of the effect of gradient field distortions. *Magn Reson Med* 2003;**50**:791-801

Table 1 – Average absolute particle trace deviations

Average absolute distance Δy and standard deviation between the endpoints of the particle traces and the seeding plane, before and after subtraction or linear background phase correction. Asterices (*) indicate statistically significant difference ($p<0.05$) from the corresponding uncorrected dataset.

	Δy [mm]			
	SENSE = 2	k-t = 2	k-t = 4	k-t = 5
Uncorrected	5.3±0.5	5.0±0.5	5.0±0.3	5.1±0.4
After subtraction	2.7±0.5 *	2.2±0.5 *	2.5±0.5 *	2.6±0.6 *
After linear background correction	1.5±0.4 *	1.3±0.4 *	1.1±0.3 *	1.3±0.6 *

* $p < 0.05$

Figure legends

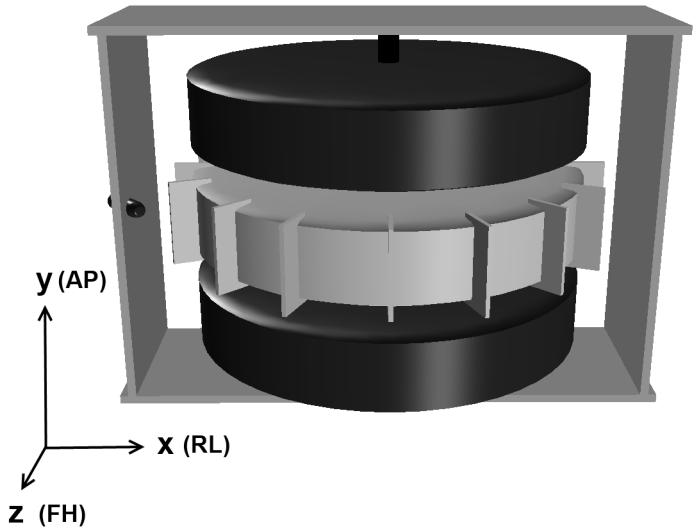

Fig. 1. The middle rotating cylinder (gray) positioned with the rotational axis along the y (Anterior-Posterior) direction. The phantom was positioned in the isocenter of the scanner, with the B_0-field aligned along the z (Feet-Head) direction. During imaging, the central disc rotated in the x-z plane. Apart from lacking plastic fins, the outer cylinders (black) were identical in size and material composition to the rotating cylinder, but were kept stationary for stabilization and as a reference for background correction.

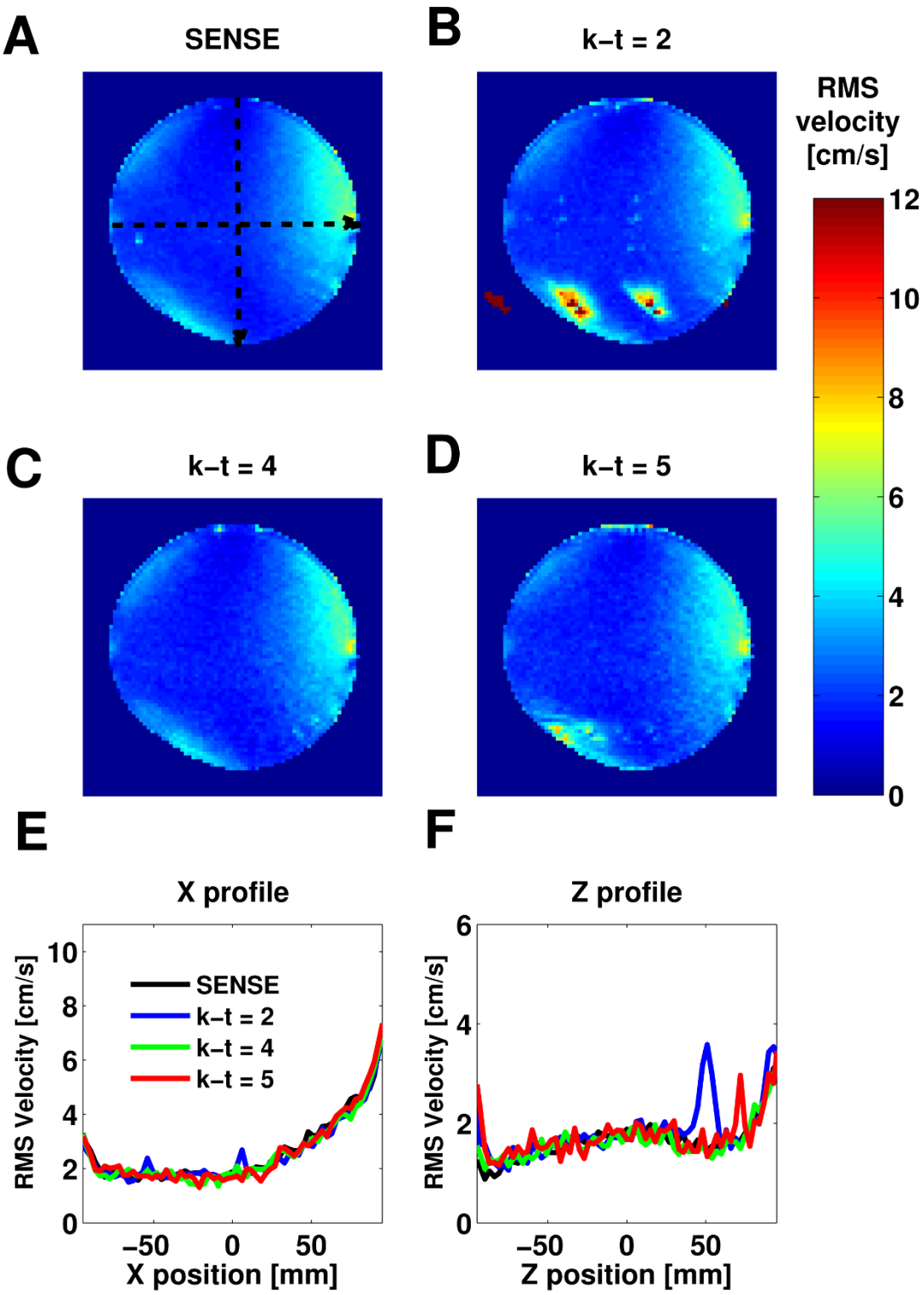

Fig. 2 RMS velocity maps of the central cylinder, acquired with the SENSE-accelerated 4D PC sequence (A) and with k-t BLAST speedup factors of 2, 4 and 5 (B-D) while the phantom was at rest. Below: RMS velocity profiles (from figures A-D, profile positions shown by

dashed arrows in A) in x- (E) and z (F) direction, respectively. The SENSE acquisition is denoted by a black line, and k-t BLAST accelerated acquisitions with speedup factors of 2, 4 and 5 by blue, green and red lines, respectively.

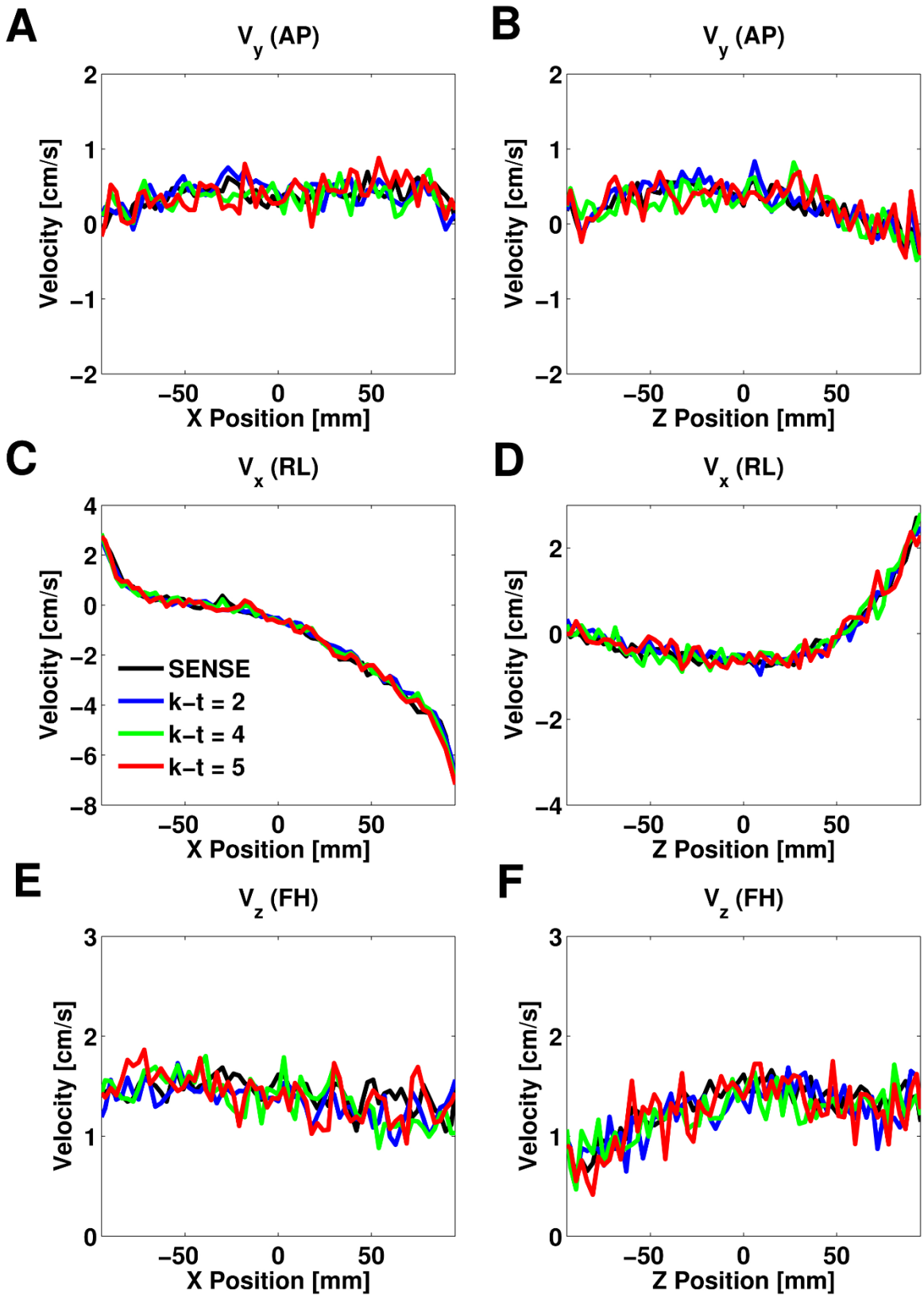
A
V_y (AP)
Velocity [cm/s]
X Position [mm]
B
V_y (AP)
Velocity [cm/s]
Z Position [mm]
C
V_x (RL)
Velocity [cm/s]
SENSE
k–t = 2
k–t = 4
k–t = 5
X Position [mm]
D
V_x (RL)
Velocity [cm/s]
Z Position [mm]
E
V_z (FH)
Velocity [cm/s]
X Position [mm]
F
V_z (FH)
Velocity [cm/s]
Z Position [mm]

Fig. 3 Velocity profiles showing the time-averaged background for the velocity components v_y (A, B), v_x (C, D) and v_z (E, F). Data was acquired with the central cylinder at rest. The profiles were positioned through the center of the phantom, as shown by dashed lines in Fig. 2A, Velocity profiles are shown for all velocity components in the x-direction (A, C, E), and in the z-direction (B, D, F). All sequences exhibit similar phase background patterns, with background velocities increasing with greater distance from the center of the FOV. The v_x velocity component (C,D) had highest velocity offsets. The SENSE acquisition is denoted by a black line, and k-t BLAST accelerated acquisitions with speedup factors of 2, 4 and 5 by blue, green and red lines, respectively.

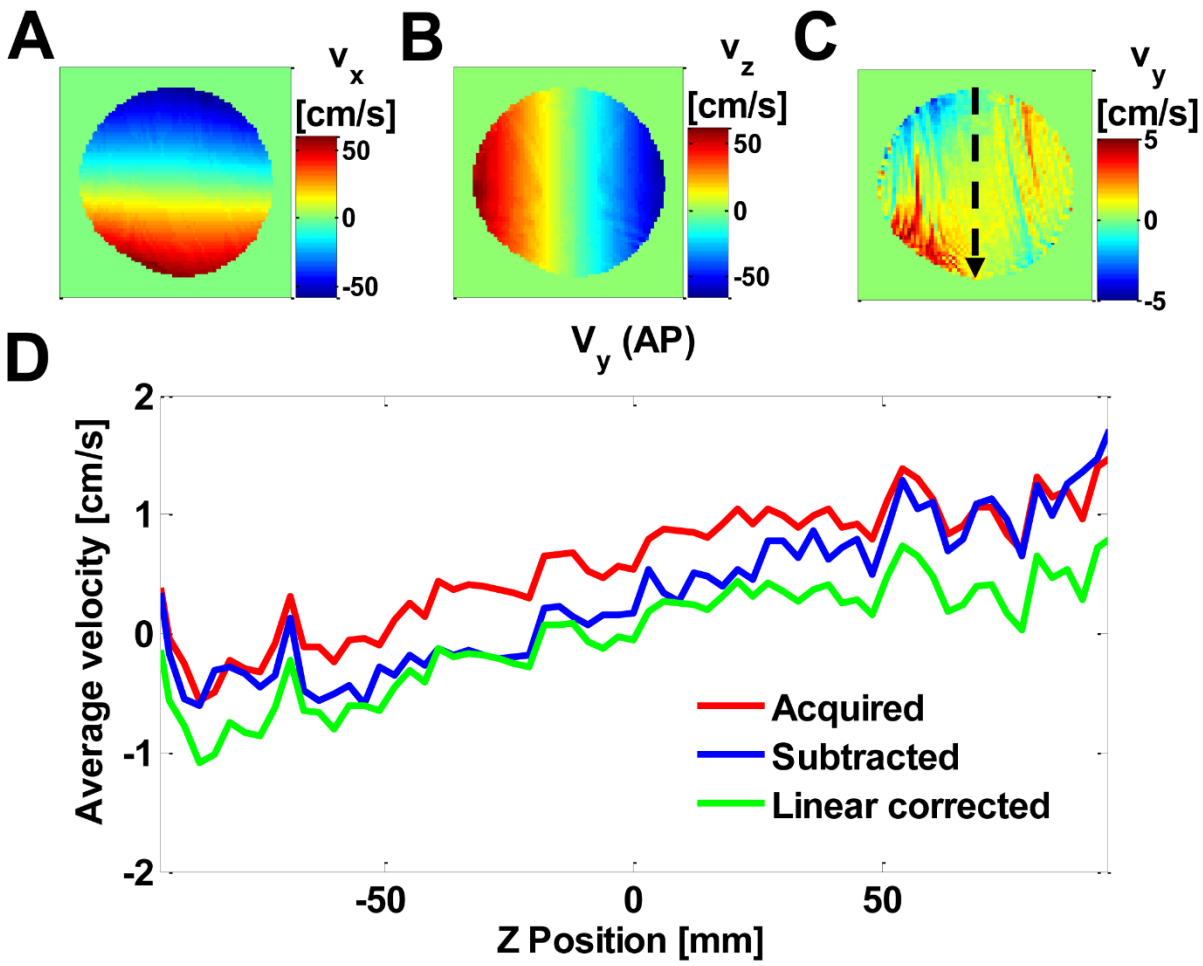

Fig. 4 Time-averaged velocity components in the central rotating cylinder acquired with the SENSE-accelerated sequence (A-C). Note that the phantom rotates in the x-z plane. The v_y

velocity component perpendicular to the rotational plane shows a spatially varying phase offset. Similar observations were seen in the datasets with k-t BLAST acceleration. Below: Line profile from the SENSE-accelerated dataset (D), presenting time-averaged velocity in y direction, perpendicular to the rotating disc (red line). The profile is placed along the dotted line in C). For comparison, the corresponding velocity profile is plotted after the measured dataset was subtracted (blue line) or linear phase corrected (green line). Note that phase correction in some parts resulted in phase offsets with opposite sign as before correction.

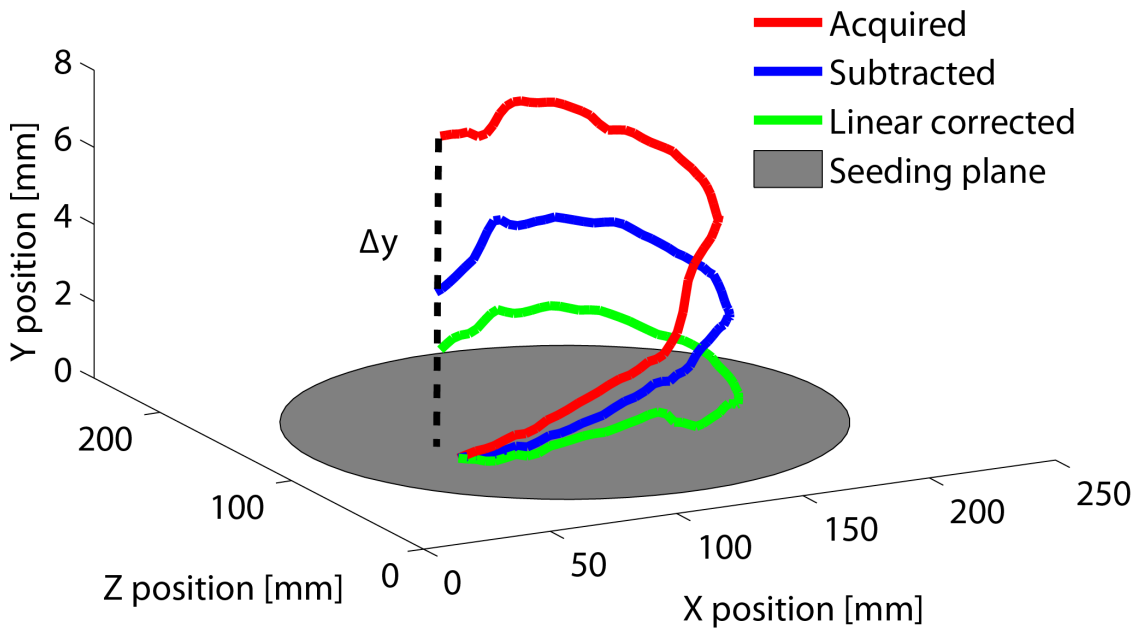

Fig. 5 Example of typical particle trace trajectories in the rotating cylinder, seeded in the center of the rotating cylinder. For the ease of interpretation only one particle trace is presented. Performing phase background correction by subtraction (blue) or linear phase correction (green) reduces the distance Δy from the reference plane (dotted line).

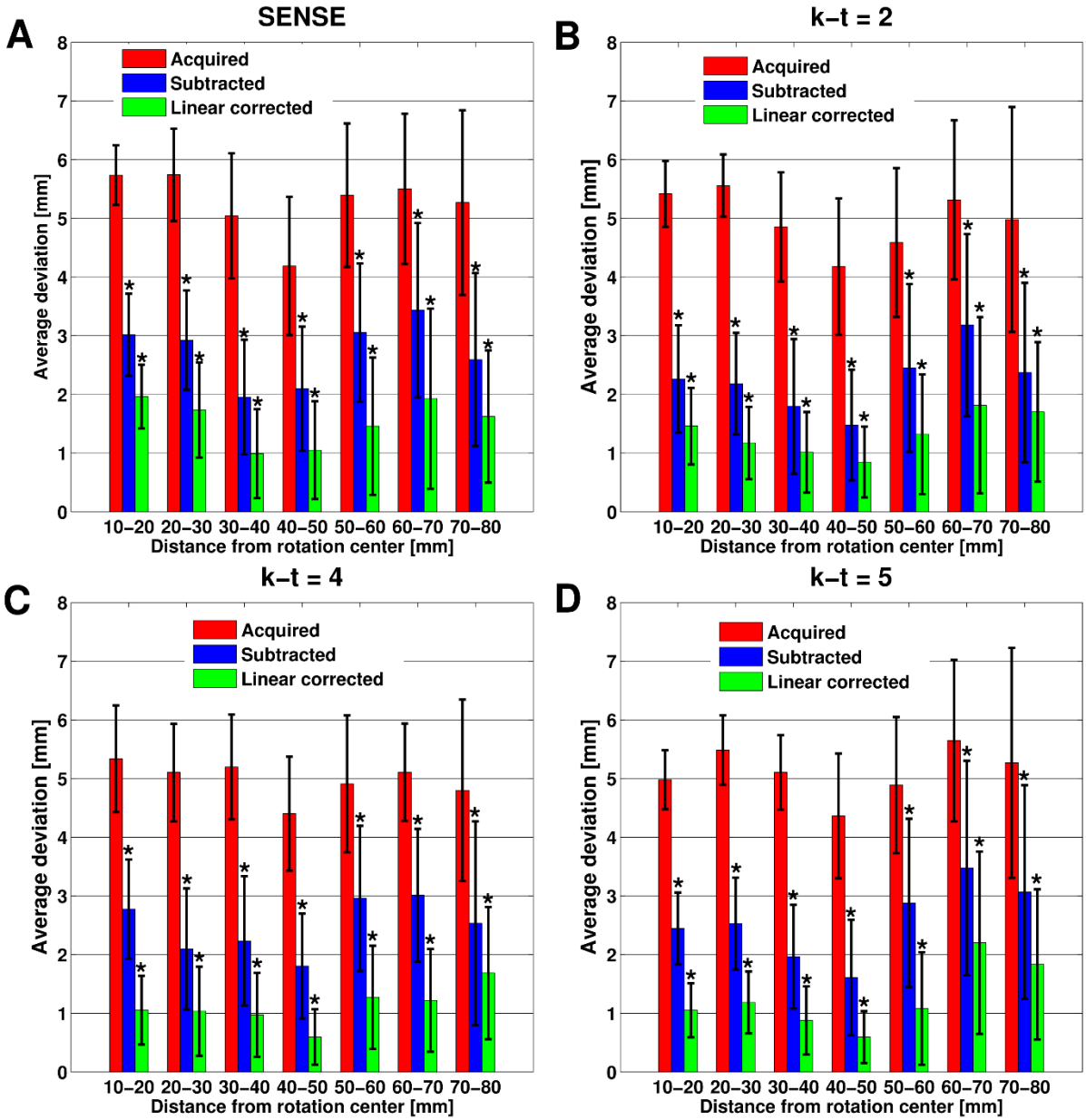

Fig. 6 Average Δy in pathline end positions, sorted by their starting distance from the rotational center of the disc in radius intervals of 10 mm width. Results are presented from the SENSE-accelerated dataset (A), and the datasets acquired with a k-t BLAST acceleration factor of 2,4 and 5 (B-D). Red bars show average Δy for the acquired velocity field, blue bars the average Δy after the measured velocity field has been subtracted with the static dataset, and green bars after first-order linear correction. Error bars represent standard deviation. Asterices indicate statistically significant difference from the corresponding uncorrected deviation ($p < 0.05$)